Combined experimental and theoretical study of the $6p\,^2P_j \rightarrow 8s\,^2S_{1/2}$ relative transition matrix elements in atomic Cs

A. Sieradzan
Physics Department, Central Michigan University, Mt. Pleasant, Michigan 48859, USA

M. D. Havey
Department of Physics, Old Dominion University, Norfolk, Virginia 23529, USA

M. S. Safronova
Electron and Optical Physics Division, National Institute of Standards and Technology, U.S. Department of Commerce, Gaithersburg, Maryland 20899-8410, USA

(Received 23 August 2003; published 6 February 2004)

A combined experimental and theoretical study of transition matrix elements of the $6p\,^2P_j \rightarrow 8s\,^2S_{1/2}$ transition in atomic Cs is reported. Measurements of the polarization-dependent two-photon excitation spectrum associated with the transition were made in an $\approx 200\ \mathrm{cm}^{-1}$ range on the low-frequency side of the $6s\,^2S_{1/2} \rightarrow 6p\,^2P_{3/2}$ resonance. The measurements depend parametrically on the relative transition matrix elements, but also are sensitive to far-off-resonance $6s\,^2S_{1/2} \rightarrow np\,^2P_j \rightarrow 8s\,^2S_{1/2}$ transitions. In addition, as the measured quantities are ratios of polarization-dependent intensities at a single-excitation frequency, they are quite insensitive to a variety of common-mode systematic effects; matrix-element ratios may then be determined to high accuracy. In the past, the matrix-element dependence has yielded a generalized sum rule, the value of which is dependent on sums of relative two-photon transition matrix elements. In the present case, best available determinations from other experiments are combined with theoretical matrix elements to extract the ratio of transition matrix elements for the $6p\,^2P_j \rightarrow 8s\,^2S_{1/2}$ ($j = 1/2, 3/2$) transition. The resulting experimental value of 1.423(2) is in excellent agreement with the theoretical value, calculated using a relativistic all-order method, of 1.425(2).

DOI: 10.1103/PhysRevA.69.022502 PACS number(s): 32.70.Cs, 32.30.Jc, 31.30.Jv

I. INTRODUCTION

Although some of the earliest experiments in atomic physics were measurements of atomic lifetimes and oscillator strengths [1,2], precise determination of atomic transition matrix elements remains a demanding enterprise [3–6]. Some perspective on this may be gained by noting that, in spite of the development of a wide array of sophisticated experimental techniques, measurements depending directly on atomic transition matrix elements seldom have achieved a precision better than $\sim 0.5\%$, this being for the deeply studied alkali-metal atoms [3–16]. Measurements made for non-alkali-metal atoms, often motivated by the need for data in some other area of atomic physics research [1,17–20], have typically cited even lower precision.

We have similarly been concerned with precise measurements in alkali-metal atoms, and we have a continuing experimental program of precision measurement of relative and absolute transition matrix elements in the one-electron atoms [21–25]. The main experimental approaches have been based either on polarization-dependent Rayleigh and Raman scattering in atomic Cs or on polarization-dependent two-photon spectroscopy applied to Na and Rb. In our approach, the main measured quantities are ratios of intensities for two different polarization states of either detection or excitation. Since the measurements are made at fixed excitation frequency, the ratios are insensitive to most experimental variables, and can be made with high accuracy. In addition, the precision is generally high, because two-photon transition rates can be quite significant in atoms and because the fluorescence signature of the excitation is nearly background-free. These advantages translate typically into a fractional measurement uncertainty on the order of 10^{-3}.

In spite of the fact that many experimental [8–13,26] and theoretical [27–32] approaches have been applied to determination of atomic properties of atomic ^{133}Cs, including lifetimes or oscillator strengths and polarizabilities, only limited higher-precision experimental data are available for many valence transition matrix elements in this atom. These studies have been motivated in part by a serious need for empirical data to extract more fundamental information from precise measurement of parity nonconservation (PNC) in this atom [33], especially in light of the discrepancy reported in Ref. [34] between values of the weak charge Q_{w} extracted from high-precision atomic physics experiment [33] and the accepted standard model value. In order to clarify the situation, recent experimental efforts have concentrated on measurement of transition matrix elements associated with the $6s$-$6p$ and $6s$-$7p$ multiplet transitions [12,13]. However, the $6p$-$7s$ and $7p$-$7s$ transitions, which are less experimentally accessible, make similarly important contributions. The availability of high-precision experimental data for any transitions between low-lying states of Cs is important for providing additional information regarding the accuracy of the theoretical calculations in Cs which is crucial for the accurate analysis of Cs PNC experiment.

In this paper we present results of our measurements of the spectral and polarization dependence of the $6s\,^2S_{1/2}$

$\rightarrow np\,^2P_j \rightarrow 8s\,^2S_{1/2}$ $(j=1/2,3/2)$ two-color, two-photon transition in ^{133}Cs, where $n=6$ is the dominant term. In an earlier report [22] we described how such measurements could be interpreted in terms of a type of sum rule related to the scalar and vector transition probabilities. The sum rule is evaluated by fitting experimental polarization-dependent spectra to a generalized form containing, as fitting parameters, the relative two-photon transition matrix elements for the contributing transitions, allowing extraction of the ratio of the matrix elements in the dominant term. The contributions from far-off-resonance transitions are small but significant for heavy atoms such as Cs and are evaluated theoretically. In the present paper we describe that approach as applied to the Cs $6s\,^2S_{1/2} \rightarrow 8s\,^2S_{1/2}$ two-photon transition. By combining the present measurements with precisely determined $6s\,^2S_{1/2} \rightarrow 6p\,^2P_j$ resonance transition matrix elements, the $6p\,^2P_j \rightarrow 8s\,^2S_{1/2}$ relative excited-state matrix elements are determined. We point out that the same combined scheme can effectively be used to determine matrix elements for the $6s\,^2S_{1/2} \rightarrow 7p\,^2P_j \rightarrow 7,\ 8s\,^2S_{1/2}$ transitions which, because of their importance for analysis of the precision parity nonconservation measurements in Cs, remain interesting cases to investigate [13].

In the following sections, we briefly review our experimental approach, with particular attention to aspects different in the present study. This is followed by a description of our experimental results and data analysis. We then describe the application of results of relativistic many-body calculations of the off-resonance terms, which allows the extraction of the desired two-photon transition matrix element ratios. Finally, the relative $6p\,^2P_j \rightarrow 8s\,^2S_{1/2}$ relative transition matrix elements are determined and compared with theoretical calculations.

II. EXPERIMENTAL APPROACH

The general experimental approach is described in previous reports [21,22,24,25], and so will only briefly be reviewed here. The basic experimental scheme [21] is illustrated in Fig. 1, which contains a partial energy-level diagram for the lowest few levels of atomic Cs. A block diagram of the experimental apparatus is shown in Fig. 2. In the experiment, atoms in the $6s\,^2S_{1/2}$ ground level are excited by two-photon absorption to the $8s\,^2S_{1/2}$ final level. In principle, all the intermediate $np\,^2P_j$ levels, including continuum terms, contribute to the total excitation probability [35]. In practice, and depending on the precision of the measurements, significant contributions are limited to the first few nearest-to-resonance terms. The first step of the excitation scheme is accomplished with an Ar^+ laser pumped Ti:sapphire laser (laser 1) tuned in a several hundred cm^{-1} energy range to the red side of the $6s\,^2S_{1/2} \rightarrow 6p\,^2P_j$ transition, which has a hyperfine-weighted transition frequency of $\omega_{3/2}=11\,732.31\ cm^{-1}$ [36,38]. With reference to Fig. 1, the detuning from one-photon resonance is defined as $\Delta=\omega_1-\omega_{3/2}$, where the laser 1 frequency is ω_1. Although detunings of magnitude greater than 200 cm^{-1} were investigated, useful data were obtained only for $|\Delta|<200\ cm^{-1}$. A Michelson-inteferometer-type wavemeter, which has a precision of 10^{-3} cm^{-1}, is used to determine ω_1. The Ti:sapphire laser is passively stabilized with a thin-thick etalon combination and has a short-term linewidth on the order of a few MHz. Long-term drifts, on a time scale longer than a typical data run of a few minutes, are dominated mainly by thermal and mechanical noise, and have a negligible influence on the experimental results. The average power is $\approx$200 mW. The laser 1 output is strongly linearly polarized, which is further purified by passing the beam through a Glan-Thompson prism polarizer. The beam is then passed through an electronically controlled liquid-crystal retardation (LCR) wave plate, which switches the linear polarization direction to one of two orthogonal linear polarization directions. The resulting variable polarization beam is then directed to the Cs sample cell. The second excitation step is driven by the linearly polarized output from an external cavity diode laser (ECDL, laser 2), which generates an average power of 8 mW in a short-term ($\sim$1 s) bandwidth $\sim$1 MHz. The laser has a

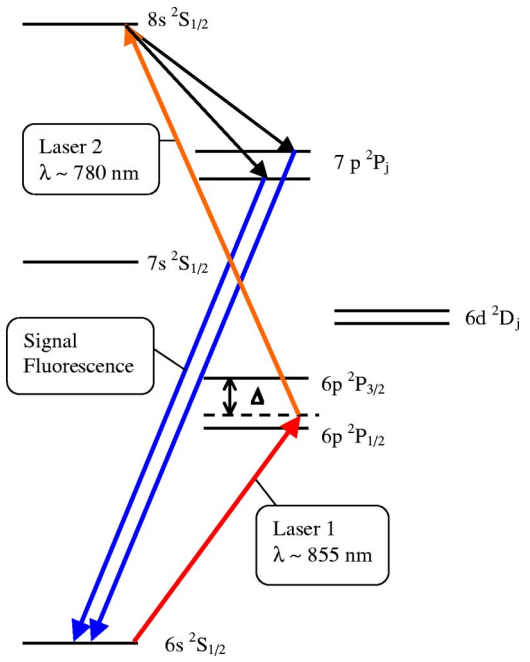

FIG. 1. Partial energy-level diagram for atomic Cs, showing the excitation scheme used in the experiment.

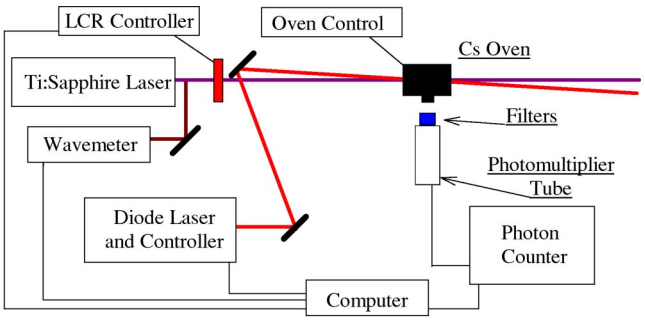

FIG. 2. Schematic diagram of the experimental apparatus, showing the layout of the main elements of the experiment. The Ti:sapphire laser is laser 1 and the diode laser is laser 2. The liquid-crystal retarder controller is labeled as the LCR controller.

frequency ω_2 which nominally satisfies the two-photon resonance condition $\omega_1+\omega_2=\omega_0$, where ω_0 is the frequency separation of hyperfine components of the $6s\,^2S_{1/2}$ and $8s\,^2S_{1/2}$ levels. The degeneracy-weighted hyperfine averaged value of $\omega_0=24\,317.17$ cm^{-1} [36]. The laser 2 frequency is determined from the detuning according to $\omega_2=\omega_0-\omega_{3/2}-\Delta$. When $\Delta=0$, the excited-state resonance frequency is $\omega_2=12\,584.82$ cm^{-1} [36]. The commercial ECDL is piezoelectrically scannable over a range of $\approx$15 GHz around the two-photon resonance. The diode laser output beam is made to be nearly collinear with that from the Ti:sapphire laser and the two beams are weakly focused with 0.5 m focal length lenses and overlapped in the central region of a sample cell assembly.

The Cs vapor cell is an evacuated and sealed Pyrex cell having a length of about 7.5 cm and a diameter of 2.5 cm. Research grade windows are fused directly onto the cell body, leaving about a 2.0 cm diameter undistorted central region for transmission of the laser beams. The cell is prepared on an oil-free vacuum system and is evacuated to a base pressure of about 10^{-8} mbar. A small amount of Cs metal is driven into the cell prior to removing it from the vacuum system. The cell temperature is varied by placing it in a resistively heated oven, which allows heating to a typical temperature of 375 K, corresponding to a Cs vapor density of about 2.6×10^{11} cm^{-3}. The cell temperature is stabilized to about ±0.1 K using a thermocouple attached to the coolest part of the cell; the thermocouple output is fed back to the oven power supply.

Two-photon resonance signals are monitored by measurement of the $7p\,^2P_j\rightarrow6s\,^2S_{1/2}$ cascade fluorescence at 455 nm and 459 nm. The fluorescence is collected at right angles to the laser beams by a short focal length field lens ($\sim$5 cm), which approximately collimates the fluorescence light on the cathode of a red-light sensitive photomultiplier tube (PMT). The tube is protected from background light and the intense laser beams by a combination of colored glass and narrow-band interference filters. Infrared transmitting colored glass filters mounted on the entrances to the oven housing further reduce background light signals. The PMT output is amplified and the photon-counting rate measured with a commercial 100 MHz photon counter. Typical counting rates on two-photon resonance are $\sim10^3$ s^{-1}. We point out that the operating temperature of 375 K turns out to be optimal for this experiment. At lower temperatures the fluorescence signals are weak, while at elevated temperatures, and correspondingly larger Cs atom density, the vapor becomes optically thick to the $7p\,^2P_j\rightarrow6s\,^2S_{1/2}$ signal radiation. Then branching to the $7s\,^2S_{1/2}$ and $6d\,^2D_j$ levels (see Fig. 1) is enhanced, and signals in the observed decay channel are correspondingly reduced.

The various instruments are globally controlled or monitored by a computerized data acquisition and instrument control program. To illustrate the experimental protocol, consider a typical experimental run, where laser 1 is set to a nominal frequency, which is measured by the wavemeter, which passes this value to the main control program. Sequentially, the photon-counting rate is measured alternately for collinear and perpendicular linear polarization directions of the two lasers. The retardance of the LCR is controlled with a specially written instrument driver that communicates with the LCR hardware via the computer parallel port. The frequency of the ECDL (laser 2) is then shifted by piezoelectrically scanning the ECDL cavity length; this is achieved by direct communication between the ECDL controller and the main experiment computer. The wavemeter reading is recorded again and the data cycle is repeated. This experimental protocol is very effective for determining the shape of the excitation line and for assessing the blending of different hyperfine components of the excitation line shape. An alternate data-taking protocol was also employed. In this, once a proper setting of laser 2 was determined, which minimized the influence of hyperfine blending on the measured polarization, the laser 2 frequency was not scanned. Data were then accumulated by switching the laser polarization until sufficient statistics were obtained.

For each data run, the experimental signal is determined for two different states of relative linear polarization of the excitation lasers. Although the absolute intensities of these components depend on many experimental factors, including the laser intensities, Cs density, and the sensitivity of the detection electronics, the intensity ratio is sensitive only to the relative polarization state of the lasers and the two-photon matrix elements. The main experimental observable for detailed analysis is then the linear polarization degree defined as

$$P_L=\frac{S_\parallel-S_\perp}{S_\parallel+S_\perp}, \tag{1}$$

where $S_\parallel$ and $S_\perp$ are the measured signal intensities when the laser beams are linearly polarized collinearly or perpendicularly, respectively.

The nuclear spin of ^{133}Cs is $I=7/2$, and so both the $6s\,^2S_{1/2}$ and $8s\,^2S_{1/2}$ electronic states have hyperfine components of total angular momentum $F=3$, 4. The hyperfine splitting in the ground $6s\,^2S_{1/2}$ level is the international frequency standard [37], which is $\approx$9.192 GHz, while the hyperfine splitting in the $8s\,^2S_{1/2}$ level is about one-tenth this value and is on the order of 0.9 GHz. Each of these splittings is larger than the one-photon Doppler width of several hundred MHz associated with the separate $6s\,^2S_{1/2}\rightarrow6p\,^2P_j$ and $6p^2P_j\rightarrow8s\,^2S_{1/2}$ transitions, and so partial resolution of the hyperfine splitting is expected even when the two excitation laser beams are copropagating through the sample cell. This is illustrated in Fig. 3, which shows the spectral and relative polarization dependence of the two-photon excitation rate at $\Delta=-80.37$ cm^{-1}. The main contribution to the spectral width is due to Doppler broadening, which is approximately double that for a one-photon transition. On the other hand, for counterpropagating beams, nearly complete cancellation of the Doppler width is expected, with a residual two-photon Doppler width $\sim$10 MHz. Such a typical scan is shown in Fig. 4, which corresponds to the $F=4\rightarrow F'=4$ transition with $\Delta=-22.0$ cm^{-1}. There it is seen that the spectral width of the line shape is $\approx$40 MHz, which corresponds well to the combined residual Doppler width and the spectral width of the Ti:sapphire laser. It is also seen that the excita-

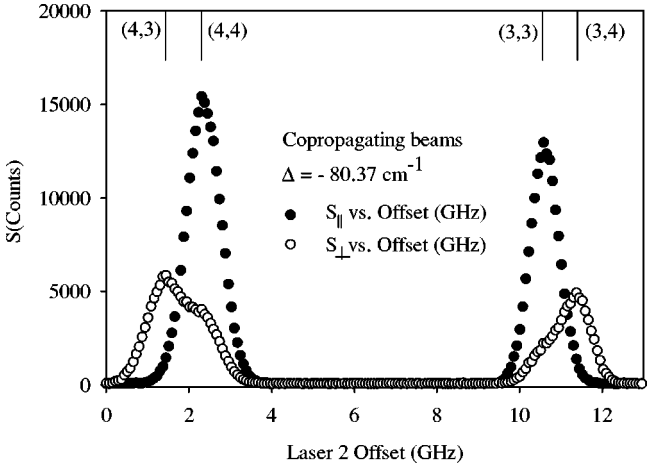

FIG. 3. Experimental signal for frequency and polarization-dependent two-photon excitation at a detuning of $-80.37\ \mathrm{cm}^{-1}$ from resonance. All four hyperfine transitions are shown, are denoted by (F,F'), and are labeled by the vertical lines above each component. The laser 2 offset is measured from a convenient starting point, denoted by the origin of the graph. Copropagating beams.

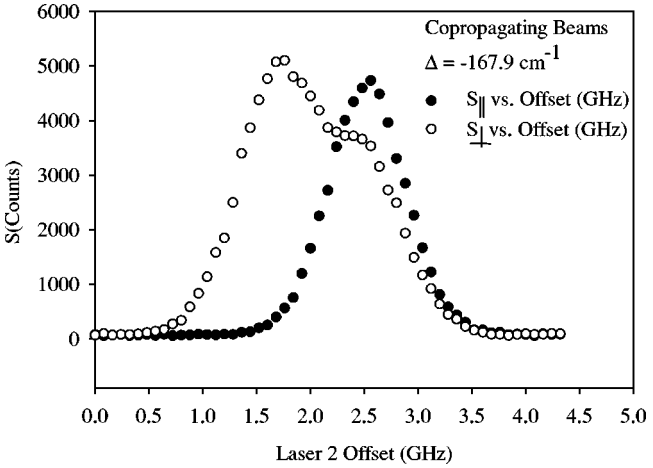

FIG. 5. Experimental signal for frequency and polarization-dependent two-photon excitation at a detuning of $-167.9\ \mathrm{cm}^{-1}$ from resonance. The $F=4\rightarrow F'=3$ and $F=4\rightarrow F'=4$ transitions are shown. The laser 2 offset is measured from a convenient starting point, denoted by the origin of the graph. Copropagating laser beams.

tion spectrum depends significantly on the relative polarization state of the two laser beams, giving in this case a large linear polarization degree of ≈ 0.78.

In spite of the evidently good signal to noise ratio for the data in Fig. 4, it proved difficult to achieve the desired reproducibility in the polarization measurements with the passively stabilized Ti:sapphire laser. The main reason for this was that measurement of the two different polarization states were made sequentially, and fluctuations in the laser frequency on the switching time scale introduced unwanted noise in the extracted polarization values. The reason for this is that when the lasers are counterpropagating through the interaction region of the cell, the Doppler width of the two-photon transition is greatly reduced, and is on the order of the natural width of the final $8s$ level. In this case, in order to obtain reliable polarization measurements, the combined frequency drift of the two lasers would need to be smaller than a fraction of 1 MHz/s. Instead, we recorded the excitation spectrum for copropagating laser beams, for which the Doppler width is large (several hundred MHz) and for which the characteristic laser frequency drift rates of a few MHz/s are entirely acceptable. Note that variation of the polarization in the few MHz range is totally negligible. The small penalty to be paid for this is that the polarization values need to be determined in the wings of the partially blended lines. However, these determinations were made sufficiently far into the wings that the other hyperfine transition made nearly negligible contribution to the polarization value. In addition, the signals were significantly less noisy than with counterpropagating beams, making possible consistent and repeatable measurements of the polarization at each detuning. A typical higher-resolution data run is presented in Fig. 5, which corresponds to the $F=4\rightarrow F'=3$, 4 transitions at $\Delta=-167.9\ \mathrm{cm}^{-1}$.

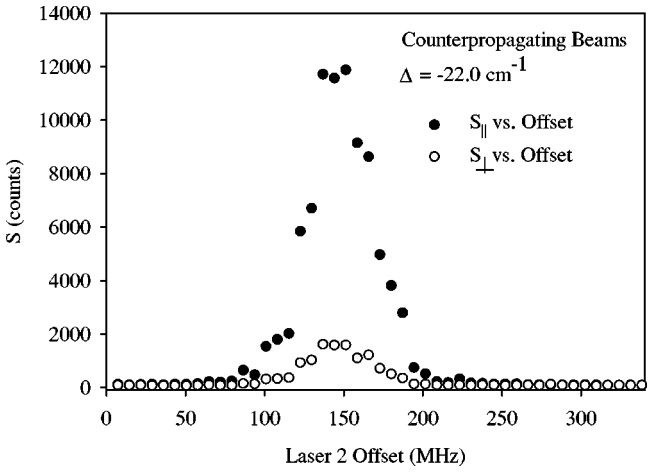

FIG. 4. Experimental signal for frequency and polarization-dependent two-photon excitation at a detuning of $-22.00\ \mathrm{cm}^{-1}$ from resonance. The $F=4\rightarrow F'=4$ transition is shown. The laser 2 offset is measured from a convenient starting point, denoted by the origin of the graph. Counterpropagating laser beams.

Finally, we have modeled the residual effect of blending of the hyperfine lines on the measured polarization values. In the model, we approximate each hyperfine transition line shape to be Gaussian and having the measured width determined by the Doppler broadening of the two-photon transition. Using the known relative hyperfine transition probabilities gives a polarization-dependent correction that ranges from 0.0005 to 0.0013 (polarization values reported here can range from -1 to $+1$). Even though these corrections are well within the statistical error associated with each measured polarization, the corrections are systematic and so are made directly to the measured counting rates, prior to extracting P_L values from the data through Eq. (1).

Analysis and experimental results

The variation of the linear polarization degree with detuning Δ of laser 1, and for each of the four electric dipole

allowed hyperfine transitions, may be readily calculated in terms of transition matrix elements (the general expression may be found in Ref. [35]). The dominant intermediate levels for the two-photon transitions are the $6p\,^2P_j$ levels, with $j=1/2,\ 3/2$, but other $np\,^2P_j$ transitions, including the p continuum, also contribute to the total transition probability, and play an important role in the experiments reported here. For the transitions when $\Delta F=\pm 1$, absorption of two photons with collinear polarization directions is forbidden, and so the linear polarization degree is -1, independent of detuning. However, for the other transition pair, where $\Delta F=0$, both fine structure multiplet components contribute, leading to strong spectral variations in the linear polarization degree. Theoretical expressions for the intensities are given by

$$I_{\parallel}=4I_{o33}\left[\frac{R}{\omega_1-\omega_{3/2}}+\frac{1}{\omega_1-\omega_{1/2}}+\frac{R}{\omega_2-\omega_{3/2}}+\frac{1}{\omega_2-\omega_{1/2}}+P\right]^2, \tag{2}$$

$$I_{\parallel}=I_{o33}\left[\frac{R/2}{\omega_1-\omega_{3/2}}-\frac{1}{\omega_1-\omega_{1/2}}-\frac{R/2}{\omega_2-\omega_{3/2}}+\frac{1}{\omega_2-\omega_{1/2}}+Q\right]^2, \tag{3}$$

for the $F=3\rightarrow F'=3$ transition and

$$I_{\parallel}=\frac{36}{15}I_{o44}\left[\frac{R}{\omega_1-\omega_{3/2}}+\frac{1}{\omega_1-\omega_{1/2}}+\frac{R}{\omega_2-\omega_{3/2}}+\frac{1}{\omega_2-\omega_{1/2}}+P\right]^2, \tag{4}$$

$$I_{\parallel}=I_{o44}\left[\frac{R/2}{\omega_1-\omega_{3/2}}-\frac{1}{\omega_1-\omega_{1/2}}-\frac{R/2}{\omega_2-\omega_{3/2}}+\frac{1}{\omega_2-\omega_{1/2}}+Q\right]^2, \tag{5}$$

for the $F=4\rightarrow F'=4$ transition. In these expressions, the overall intensity for each hyperfine transition is proportional to $I_{oFF'}$, while R, P, and Q are parameters that are proportional to ratios of reduced transition matrix elements [39]. In the present case,

$$R=\frac{\langle 8s\|d\|6p_{3/2}\rangle\langle 6p_{3/2}\|d\|6s\rangle}{\langle 8s\|d\|6p_{1/2}\rangle\langle 6p_{1/2}\|d\|6s\rangle}, \tag{6}$$

where d is the electric dipole operator. The quantities P and Q are given by

$$P=\sum_{n>6,jk}\frac{M_{njk}}{\omega_k-\omega_{np_j}}, \tag{7}$$

$$Q=\sum_{n>6,jk}\frac{(-1)^{j+1/2}}{j+1/2}\frac{M_{njk}}{\omega_k-\omega_{np_j}}, \tag{8}$$

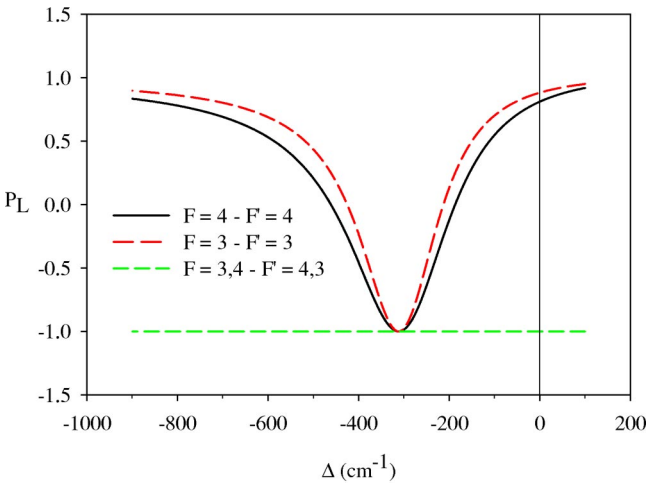

FIG. 6. Model dependence of the variation of the linear polarization degree with detuning from resonance for all four permitted hyperfine transitions. The matrix-element ratio is taken to be $R=2$, and contributions from far-off-resonance transitions are neglected.

where the matrix-element ratio is given by

$$M_{njk}=\frac{\langle 8s\|d\|np_j\rangle\langle np_j\|d\|6s\rangle}{\langle 8s\|d\|6p_{1/2}\rangle\langle 6p_{1/2}\|d\|6s\rangle}. \tag{9}$$

The total angular momentum $j=1/2,3/2$, while $k=1,2$ labels the frequency of the absorbed photons.

An illustration of the variation of the polarization with detuning Δ is shown in Fig. 6 for each of the four hyperfine transitions. In these plots we have taken $R=2$, corresponding to no relativistic modification of the reduced transition dipole matrix elements, and $P=Q=0$, which applies to the case when only the $n=6$ intermediate levels are considered. Among the critical features of the plots are the resonance values of the linear polarization degree for each hyperfine transition. In the present case, these values are $P_L=0.882$ for the $F=4\rightarrow F'=4$ transition and $P_L=0.811$ for the $F=3\rightarrow F'=3$ transition. In addition, there is a detuning from resonance where the polarization is $P_L=-1.0$, corresponding to the cases when the intensity $S_{\parallel}=0$ for each hyperfine transition. The location of this point generally depends on the four main terms in Eqs. (2)–(8), and on the values for P and Q.

Polarization measurements have been made in an $\approx 200\ \mathrm{cm}^{-1}$ range of detunings to the low-frequency side of the atomic $6s\,^2S_{1/2}\rightarrow 6p\,^2P_j$ resonance transition. These measurements, which have a typical one standard deviation uncertainty of 0.002, are presented in Fig. 7. The solid curves in this figure are expanded versions of those in Fig. 6. Note that the error bars on the experimental data points are negligible on the scale of the figure. It can be seen from the curves that there is significant discrepancy between the measurements and the theoretical curves (with $P=0$, $Q=0$, and $R=2$) for the $F=4\rightarrow F'=4$ transition, for which we have taken the most extensive data. At the largest detuning, this amounts to about 20 standard deviations. The departure has two main contributions, these being the fact that nonresonant

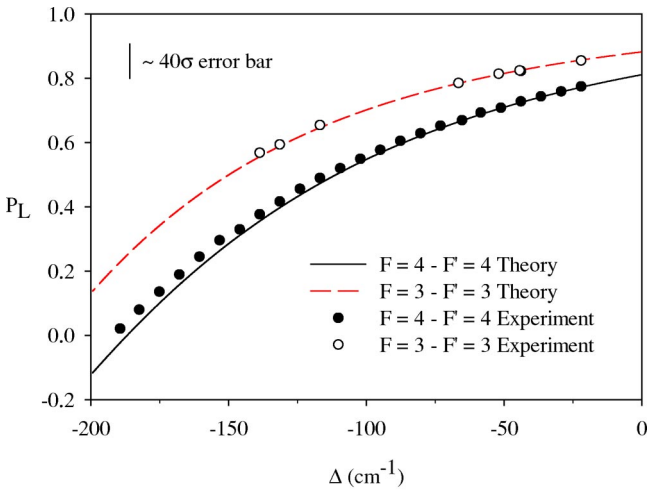

FIG. 7. Measured linear polarization degree of the two-photon excitation rate as a function of detuning for the $F=3\rightarrow F'=3$ and $F=4\rightarrow F'=4$ transitions. The solid curves represent the model curves for a matrix-element ratio $R=2$, and neglecting far-off-resonance transitions ($P=Q=0$).

transitions with $n>6$ make a significant contribution through nonzero values of P and Q, and because the value of R generally departs from the nonrelativistic value of $R=2$. In previous work, the three parameters P, Q, and R were considered as constants, which is quite well justified by their weak dependence on detuning. Fits to the detuning-dependent polarization data then yielded linear relationships among the parameters; estimates of P and Q further allowed extraction of a quite precise value for the constant matrix-element ratio R. Although this is found to be insufficient for the precision of the data presented here, we report here our values, making the same assumptions as in earlier work. That approach yields $R=2.1068(36)+443.2(1.2)P-362(362)Q$, where the uncertainty (in parentheses) in the numerical values represents one standard deviation. Note that although the coefficient of Q has an uncertainty on the order of its value, its value is correlated with that of R and P, and so it cannot be neglected. The final uncertainty in R derived from calculated values of P and Q shows that the correction due to Q is on the order of the uncertainty in R. This equation represents the equivalent sum rule to those presented in earlier reports on our measurements in Rb.

However, P and Q depend weakly on detuning, and so to obtain the highest precision it is desirable to calculate P and Q as a function of detuning directly from the most accurate experimental and theoretical matrix elements. We use a combination of the most reliable experimental and theoretical values for dominant contributions with $n\leqslant 9$. For $n=6$, measured resonance line ($n=6$) matrix elements of Rafac *et al.* [12] are employed, while for the second resonance doublet ($n=7$), we use the recently reported precision measurements of Vasilyev *et al.* [13]. Other values having $n\leqslant 9$ are obtained from the relativistic all-order calculations of Safronova *et al.* [30]; these are listed in Table I. For multiplets with $n>9$, which make only a small overall contribution to R, we use Dirac-Hartree-Fock matrix elements [28]; these values are also summarized in Table I, along with the energies associated with each intermediate np level. For reference, it is found that P and Q, calculated with these values, are fit very well by second order polynomials in detuning $\Delta=\omega_1-\omega_{10}$, and are given by $P=-2.437\times10^{-4}+3.257\times10^{-9}\Delta-3.8847\times10^{-12}\Delta^2$ and by $Q=3.260\times10^{-6}-7.683\times10^{-9}\Delta+1.645\times10^{-13}\Delta^2$. The detuning Δ is in vacuum cm^{-1} units. We estimate the total uncertainty in P and Q to be on the order of 1%.

TABLE I. Energy and matrix elements (ME) used in calculating the contributions of far-off-resonance transitions to the measured linear polarization spectrum. ME for $n\geqslant 10$ are obtained from Dirac-Hartree-Fock calculations.

np_j level	Energy (cm^{-1})	$6s$-np_j (a.u.)	$8s$-np_j (a.u.)
$6p_{1/2}$	11178.2	4.489[a]	−1.027[d]
$6p_{3/2}$	11732.4	6.324[a]	−1.462[d]
$7p_{1/2}$	21732.4	0.276[b]	−9.251[d]
$7p_{3/2}$	21765.7	0.586[b]	−14.00[d]
$8p_{1/2}$	25709.1	0.081[c]	17.71[d]
$8p_{3/2}$	25791.8	0.218[c]	24.46[d]
$9p_{1/2}$	27637.3	0.043[b]	1.743[d]
$9p_{3/2}$	27682.0	0.127[b]	2.969[d]
$10p_{1/2}$	28727.1	0.047	0.634
$10p_{3/2}$	28753.9	0.114	1.158
$11p_{1/2}$	29403.7	0.034	0.348
$11p_{3/2}$	29421.1	0.085	0.667
$12p_{1/2}$	29852.9	0.026	0.228
$12p_{3/2}$	29864.7	0.067	0.451
$13p_{1/2}$	30166.0	0.021	0.165
$13p_{3/2}$	30174.5	0.055	0.334
$14p_{1/2}$	30393.2	0.017	0.127
$14p_{3/2}$	30399.5	0.046	0.262
$15p_{1/2}$	30563.3	0.015	0.102
$15p_{3/2}$	30568.0	0.039	0.213

[a]Rafac *et al.* [12].
[b]Vasilyev *et al.* [13].
[c]Safronova *et al.* [30].
[d]This work (all order).

To obtain the matrix-element ratio defined in Eq. (6), a nonlinear least-squares fit of the polarization data of Fig. 7 is made to the theoretical expressions, using the calculated values of P and Q for each detuning. The result of the fit is $R=2.0024$ (24), where the dominant error in R comes from the statistical uncertainty in the measured polarization. The quality of the fit is illustrated in Fig. 8. In the figure, measurements are compared to the deviation of the polarization from the values obtained when $R=2$, $P=Q=0$; these are represented by the horizontal line passing through zero deviation. The experimental measurements, represented by the data points, are seen to be in excellent agreement with the solid curve, this being calculated from the fitting parameters.

The ratio of excited-state dipole matrix elements $R_{8s\text{-}6p}=\langle 8s\|d\|6p_{3/2}\rangle/\langle 8s\|d\|6p_{1/2}\rangle$ may be obtained from Eq. (6) by combining the measured value of R with the high-precision $6p$ resonance line matrix-element ratio of 1.4074(3) measured by Rafac *et al.* [11]. This gives the

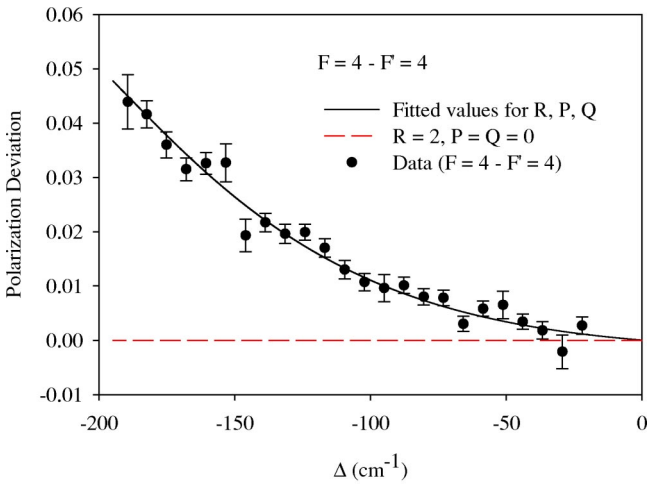

FIG. 8. Deviation of the measured linear polarization degree of the two-photon excitation rate as a function of detuning for the $F=4\rightarrow F'=4$ transition. The solid curve through the data points represents the best fit to the experimental data, while the horizontal line is the model curve result. Note that the vertical scale is magnified 20 times in comparison to Figs. 6 and 7.

excited-state matrix-element ratio of $R_{8s\text{-}6p}=1.423(2)$, which has the uncertainty of about 0.15%, with roughly equal contributions from statistical uncertainty in the measurements reported here and from the resonance line matrix-element ratio of Ref. [11]. Finally, we point out that the analysis may be reversed, if it is assumed that the bare transition matrix-element ratio is calculated precisely. Then, by recognizing that the off-resonance terms represented by P and Q contribute an average of about $-0.1091(37)$ to the value of R, the measurements determine the much smaller combination of dipole matrix elements in Eqs. (7) and (8) to about 3%. As these terms are dominated by transitions through the $6s$-$7p$ and $6s$-$8p$ multiplets, the measurements serve as a consistency check on existing measurements [13] at that level.

III. RELATIVISTIC ALL-ORDER CALCULATION OF TRANSITION MATRIX ELEMENTS

In order to compare the experimental result $R_{8s\text{-}6p}=1.423(2)$ with the high-precision theoretical value, we carry out relativistic all-order calculation of electric dipole matrix elements in Cs. In particular, we calculate $8s-np$, $n=6$, 7, 8, 9 electric dipole reduced matrix elements using a relativistic all-order method including single and double (SD) excitations [28]. The resulting values of the $8s$-$7p$, $8s$-$8p$, and $8s$-$9p$ electric dipole matrix elements were used to determine P and Q.

In the SD all-order method, the wave function of the valence electron v is represented as an expansion,

$$|\Psi_v\rangle=\left[1+\sum_{ma}\rho_{ma}a_m^\dagger a_a+\frac{1}{2}\sum_{mnab}\rho_{mnab}a_m^\dagger a_n^\dagger a_b a_a+\sum_{m\neq v}\rho_{mv}a_m^\dagger a_v+\sum_{mna}\rho_{mnva}a_m^\dagger a_n^\dagger a_a a_v\right]|\Phi_v\rangle. \tag{10}$$

TABLE II. Contributions to SD all-order electric dipole $8s$-$6p$ matrix elements in Cs. Matrix elements are given in a.u.

Contribution	$8s$-$6p_{1/2}$	$8s$-$6p_{3/2}$
DHF	1.0584	1.5145
$Z^{(a)}$	0.0173	0.0177
$Z^{(c)}$	−0.1122	−0.1606
$Z^{(d)}$	0.0938	0.1317
Z_{other}	−0.0084	−0.0108
Z_{norm}	−0.0228	−0.0308
Total	1.0260	1.4618

In this equation $|\Phi_v\rangle$ is the lowest-order atomic state wave function, which is taken to be the frozen-core Dirac-Hartree-Fock (DHF) wave function of a state v, and $a_i^\dagger$ and a_i are creation and annihilation operators, respectively. The indices a, b designate core electrons and indices m, n designate any states above the core. The equations for excitations coefficients ρ_{ma}, ρ_{mv}, ρ_{mnab}, and ρ_{mnva} are obtained by substituting the wave function Ψ_v into the many-body Schrödinger equation

$$H|\Psi_v\rangle=E|\Psi_v\rangle, \tag{11}$$

where H is the relativistic *no-pair* Hamiltonian [29]. The equations are solved iteratively until the corresponding correlation energy for the state v is sufficiently converged. The resulting excitation coefficients are then used to calculate matrix elements. The one-body matrix element of the operator Z given by

$$Z_{wv}=\frac{\langle\Psi_w|Z|\Psi_v\rangle}{\sqrt{\langle\Psi_v|\Psi_v\rangle\langle\Psi_w|\Psi_w\rangle}} \tag{12}$$

and is expressed in terms of excitation coefficients as

$$Z_{wv}=\frac{z_{wv}+Z^{(a)}+\cdots+Z^{(t)}}{\sqrt{(1+N_v)(1+N_w)}}, \tag{13}$$

where z_{wv} is the lowest-order DHF matrix element, the terms $Z^{(k)}$, $k=a\cdots t$ are linear or quadratic functions of the excitation coefficients, and normalization terms N_v are quadratic functions of the excitation coefficients. As a result, certain sets of many-body perturbation theory (MBPT) terms are summed to all orders. This method is shown to yield high-accuracy results for the primary transition electric dipole matrix elements in alkali-metal atoms [29,30,27]. The results for the reduced electric dipole matrix elements for $8s$-$6p$, $8s$-$7p$, $8s-8p$, and $8s$-$9p$ transitions are listed in Table I.

Next, we investigate the effect of the correlation to the $8s$-$6p$ matrix elements to evaluate the uncertainty of their ratio. We find that the total correlation correction to the $8s$-$6p$ matrix elements is small, 3%. However, it actually results from severe cancellations of large contributions illustrated in Table II where we give the breakdown of the all-order SD calculation for both $8s$-$6p$ transitions. The lowest-

TABLE III. Electric dipole $8s$-$6p_j$ reduced matrix elements in Cs calculated using different approximations: Dirac-Hartree-Fock (DHF), third-order many-body perturbation theory (III), single-double all-order method (SD), single-double all-order method including partial triple contributions (SDpT), and the corresponding scaled values. $R_{8s\text{-}6p}$ is the ratio of the $8s$-$6p_{3/2}$ and $8s$-$6p_{1/2}$ matrix elements. Absolute values of the matrix elements in a.u. are given.

		Ab initio			Scaled		
Level	DHF	III	SD	SDpT	III_{sc}	SD_{sc}	SDpT_{sc}
$j=1/2$	1.0584	1.0231	1.0260	1.0321	1.0315	1.0223	1.0327
$j=3/2$	1.5145	1.4519	1.4618	1.4709	1.4712	1.4556	1.4705
$R_{8s\text{-}6p}$	1.4309	1.4191	1.4247	1.4252	1.4262	1.4238	1.4240

order (DHF) value is listed in the first row of Table II. Three larger terms, $Z^{(a)}$, $Z^{(c)}$, and $Z^{(d)}$,

$$Z^{(a)}=\sum_{ma} z_{am}\tilde{\rho}_{wmva}+\sum_{ma} z_{ma}\tilde{\rho}^{*}_{vmwa},$$

$$Z^{(c)}=\sum_{m} z_{wm}\rho_{mv}+\sum_{m} z_{mv}\rho^{*}_{mw},$$

$$Z^{(d)}=\sum_{mn} z_{mn}\rho^{*}_{mw}\rho_{nv}, \tag{14}$$

where

$$\tilde{\rho}_{wmva}=\rho_{wmva}-\rho_{wmav} \tag{15}$$

are listed separately and all other terms are summed together as Z_{other}. The total normalization correction Z_{norm} defined as

$$Z_{\text{norm}}=Z_{wv}-[z_{wv}+Z^{(a)}+\cdots+Z^{(t)}] \tag{16}$$

is given separately. We find that two dominant terms, $Z^{(c)}$ and $Z^{(d)}$, nearly cancel each other and their sum almost exactly cancels out the term $Z^{(a)}$.

We note that while terms $Z^{(a)}$ and $Z^{(c)}$ contain third-order terms as well as higher-order terms (see Ref. [27] for details) the $Z^{(d)}$ term, being quadratic in valence single-excitation coefficients ρ_{mv}, contains only terms starting from fifth order. Out of the remaining terms, the largest contribution comes from the normalization correction. For these transitions, the dominant contribution to $N_{v(w)}$ in the denominator of Eq. (13) comes from the term

$$\sum_{m} \rho^{*}_{mv}\rho_{mv}. \tag{17}$$

This term contributes 97% to the N_{8s} value and 64% to the N_{6p} value. Again, this term is quadratic in single-excitation coefficients ρ_{mv} and can contain only MBPT terms starting from fifth order. Thus, $8s$-$6p$ matrix elements present an interesting case with large, but canceling, contributions from high orders in many-body perturbation theory. This cancellation occurs for both $8s$-$6p_{1/2}$ and $8s$-$6p_{3/2}$ matrix elements.

To evaluate the uncertainty in the theoretical ratio $R_{8s\text{-}6p}$ we also calculate $8s$-$6p_{3/2}$ and $8s$-$6p_{1/2}$ electric dipole matrix elements in different approximations and estimate some omitted contributions. The results are summarized in Table III. The lowest-order DHF values are listed in column labeled DHF. The results of the third-order many-body perturbation-theory calculation, which includes higher-order random-phase-approximation terms as described in Ref. [31], are listed in column "III." The third-order values, which include an estimate of the omitted fourth- and higher-order Brueckner-orbital (see classification and formulas in Ref. [31]) corrections obtained by the scaling procedure described in Ref. [31], are listed in column "III_{sc}." Single-double all-order data from Table I are listed in column "SD." The results obtained by including partial contribution of the triple excitations are listed in column labeled "SDpT." These data are obtained by adding a triple-excitation valence term to Eq. (10) and making corresponding corrections to correlation energy and single-valence excitation coefficient equations ρ_{mv} as described in Refs. [27,29,30]. The ρ_{mv} excitation coefficients give rise to the largest terms, $Z^{(c)}$ and $Z^{(d)}$, and the dominant part of N_v.

All-order SD and SDpT calculations include a complete third-order contribution (see [27] for a detailed comparison) but omit some classes of higher-order terms starting from fourth order. We have estimated some omitted correlation corrections resulting from triple and higher excitations using the scaling described, for example, in Ref. [29]. Briefly, single-particle excitation coefficients ρ_{mv} are multiplied by the ratio of the experimental and theoretical correlation energies. The modified excitation coefficients are then used to recalculate matrix elements. Such scaling estimates only certain classes of the omitted contributions (mainly Brueckner-orbital contributions, see Ref. [29] for classification of the perturbation theory terms). The corresponding SD and SDpT scaled values are listed in columns "SD_{sc}" and "SDpT_{sc}." *Ab initio* and scaled values are grouped together.

The third-order matrix elements do not differ significantly from the all-order results indicating very accurate cancellation between large higher-order terms. The Brueckner-orbital correction is dominant in a third-order calculation for both transitions and is relatively more important for the $8s$-$6p_{3/2}$ transition, thus giving a ratio differing from more accurate SD all-order value by 0.6%. We note that the ratio of the scaled third-order values, which includes an estimate of higher-order Brueckner-orbital terms, agrees with the all-order result. As one can see from Table III, the total correlation correction contribution to the ratio $R_{8s\text{-}6p}$ is very small, 0.4%, owing to the cancellation of dominant terms. The dif-

ference between all-order data in different approximations is only 0.1%. As the largest contributions to these matrix elements contain valence single-excitation coefficients ρ_{mv} the inclusion of the partial triple contributions and the scaling described above should give a good estimate of the omitted higher-order terms as both these methods are aimed at correcting ρ_{mv}. We recommend the SD *ab initio* value $R_{8s\text{-}6p}=1.425(2)$ as the final theoretical value for the ratio. The uncertainty is obtained by combining the uncertainty of the dominant terms, determined to be 0.1% based on the spread of SD, SDpT, and scaled values, and the total uncertainty in all other, much smaller, contributions taken to be 0.1% not to exceed the uncertainty of the dominant terms.

IV. DISCUSSION OF RESULTS AND CONCLUSIONS

Comparison of the theoretical matrix-element ratio of $R=1.425(2)$, and the corresponding experimental result of $R=1.423(2)$ shows excellent agreement. This is remarkable, given the various contributing theoretical and experimental factors that significantly affect the final result in each case. It is interesting to reiterate that many of the two-photon transition matrix elements in heavy alkali-metal atoms show significant relativistic modification. For example, the $5s\,^2S_{1/2}\rightarrow 5p\,^2P_j\rightarrow 5d\,^2D_{3/2}$ transition in Rb shows such variations at a level of nearly 7%. At the same time, other ratios, such as that measured in the present case, show significantly smaller relativistic modification, and yet in each case such modifications are generally well described by the highest-level atomic structure calculations. Nevertheless, there is a significant sensitivity in the experimental measurements to other dipole transitions, and these transitions depend significantly on relativistic contributions. Naturally, it would be of interest to measure the absolute oscillator strengths of the individual multiplet transitions, in order to make direct comparison of the matrix-element values reported here. Such measurements remain a significant challenge to experimental technique. Finally, the excited-state transitions in atomic Cs associated with the $7p$ doublet are of particular interest, as those second resonance line matrix elements show nearly a factor-of-2 departure from the expected line strength ratio of 2.

In conclusion, we have used precision two-photon polarization spectroscopy to make measurements of the transition matrix element ratio associated with the $6s\,^2S_{1/2}\rightarrow np\,^2P_j\rightarrow 8s\,^2S_{1/2}$ transition in atomic Cs. The measurements are combined with other experimental data and calculations in order to extract the ratio of excited-state matrix elements. The experimental value is found to be in excellent agreement with the ratio of reduced matrix elements calculated using a relativistic all-order method.

ACKNOWLEDGMENTS

The financial support of the National Science Foundation (Grant No. NSF-PHY-0099587) and Central Michigan University is greatly appreciated.

[1] F. Molish and B.P. Oehry, *Radiation Trapping in Atomic Vapours* (Clarendon Press, Oxford, 1998); Alan Corney, *Atomic and Laser Spectroscopy* (Clarendon Press, Oxford, 1998).
[2] W.L. Wiese, M.W. Smith, and B.M. Glennon, *Atomic Transition Probabilities*, Natl. Bur. Stand. (U.S.) Circ. No. 4 (U.S. GPO, Washington, D.C., 1966), Vols. 1 and 2.
[3] W.I. McAlexander, E.R.I. Abraham, and R.G. Hulet, Phys. Rev. A **54**, R5 (1996).
[4] W.I. McAlexander, E.R.I. Abraham, N.W.M. Ritchie, C.J. Williams, H.T.C. Stoof, and R.G. Hulet, Phys. Rev. A **51**, R871 (1995).
[5] C.W. Oates, K.R. Vogel, and J.L. Hall, Phys. Rev. Lett. **76**, 2866 (1996).
[6] U. Volz, M. Majerus, H. Liebel, A. Schmitt, and H. Schmoranzer, Phys. Rev. Lett. **76**, 2862 (1996).
[7] U. Volz and H. Schmoranzer, Phys. Scr. **T65**, 48 (1996).
[8] C.E. Tanner, A.E. Livingston, R.J. Rafac, F.G. Serpa, K.W. Kukla, H.G. Berry, L. Young, and C.A. Kurtz, Phys. Rev. Lett. **69**, 2765 (1992).
[9] R.J. Rafac, C.E. Tanner, A.E. Livingston, K.W. Kukla, H.G. Berry, and C.A. Kurtz, Phys. Rev. A **50**, R1976 (1994).
[10] L. Young, W.T. Hill III, S.J. Sibener, Stephen D. Price, C.E. Tanner, C.E. Wieman, and Stephen R. Leone, Phys. Rev. A **50**, 2174 (1994).
[11] R.J. Rafac and C.E. Tanner, Phys. Rev. A **58**, 1087 (1998).
[12] R.J. Rafac, C.E. Tanner, A.E. Livingston, and H.G. Berry, Phys. Rev. A **60**, 3648 (1999).
[13] A.A. Vasilyev, I.M. Savukov, M.S. Safronova, and H.G. Berry, Phys. Rev. A **66**, 020101 (2002).
[14] C.R. Ekstrom, J. Schmiedmayer, M.S. Chapman, T.D. Hammond, and D.E. Pritchard, Phys. Rev. A **51**, 3883 (1995).
[15] K.M. Jones, P.S. Julienne, P.D. Lett, W.D. Phillips, E. Tiesinga, and C.J. Williams, Europhys. Lett. **35**, 85 (1996).
[16] H. Wang, J. Li, X.T. Wang, C.J. Williams, P.L. Gould, and W.C. Stwalley, Phys. Rev. A **55**, R1569 (1997).
[17] A.A. Radzig and B.M. Smirnov, *Reference Data on Atoms, Molecules and Ions* (Springer, Berlin, 1985).
[18] C. Cohen-Tannoudji, J. Dupont-Roc, and G. Grynberg, *Atom-Photon Interactions: Basic Processes and Applications* (Wiley, New York, 1992).
[19] Harold J. Metcalf and Peter van der Straten, *Laser Cooling and Trapping* (Springer-Verlag New York, 1999).
[20] D. Mihalas, *Stellar Atmospheres* (Freeman, San Francisco, 1970).
[21] A.I. Beger, M.D. Havey, and R.P. Meyer, Phys. Rev. A **55**, 3780 (1997).
[22] R.P. Meyer, A.I. Beger, and M.D. Havey, Phys. Rev. A **55**, 230 (1997).
[23] M.D. Havey, Phys. Lett. A **240**, 219 (1998).
[24] S.B. Bayram, M. Havey, M. Rosu, A. Sieradzan, A. Derevianko, and W.R. Johnson, Phys. Rev. A **61**, 050502(R) (2000).
[25] A. Markhotok, S.B. Bayram, A. Sieradzan, and M.D. Havey, J. Appl. Phys. **92**, 1613 (2002).

[26] S.C. Bennett, J.L. Roberts, and C.E. Wieman, Phys. Rev. A **59**, R16 (1999).
[27] M.S. Safronova, Ph.D. thesis, University of Notre Dame, 2000 (unpublished).
[28] S.A. Blundell, W.R. Johnson, Z.W. Liu, and J. Sapirstein, Phys. Rev. A **40**, 2233 (1989).
[29] S.A. Blundell, W.R. Johnson, and J. Sapirstein, Phys. Rev. A **43**, 3407 (1991).
[30] M.S. Safronova, W.R. Johnson, and A. Derevianko, Phys. Rev. A **60**, 4476 (1999).
[31] W.R. Johnson, Z.W. Lui, and J. Sapirstein, At. Data Nucl. Data Tables **40**, 2233 (1989); *ibid.* **64**, 279 (1996).
[32] V.A. Dzuba, V.V. Flambaum, and O.P. Sushkov, Phys. Lett. A **142**, 373 (1989).
[33] C.S. Wood, S.C. Bennett, D. Cho, B.P. Masterson, J.L. Roberts, and C.E. Tanner, Science **275**, 1759 (1997).
[34] S.C. Bennett and C.E. Wieman, Phys. Rev. Lett. **82**, 2484 (1999).
[35] R. Louden, *Quantum Theory of Light*, 2nd ed. (Oxford University Press, Oxford, 1992).
[36] C.E. Moore, Atomic Energy Levels, Natl. Bur. Stand. (U.S.) Circ. No. 35 (U.S. GPO, Washington, D.C., 1971).
[37] Bureau Internationale des Poids et Measures, Pavillon de Breteuil, 92312 Svres Cedex, France.
[38] Th. Udem, J. Reichert, T.W. Hänsch, and M. Kourogi, Phys. Rev. A **62**, 031801 (2000).
[39] M.E. Rose, *Elementary Theory of Angular Momentum* (Wiley, New York, 1957).